Pure Appl. Geophys. 170 (2013), 815–830

DOI 10.1007/s00024-012-0585-2

Pure and Applied Geophysics

Waveform Retrieval and Phase Identification for Seismic Data from the CASS Experiment

Zhiwei Li,[1] Qingyu You,[2] Sidao Ni,[1] Tianyao Hao,[2] Hongti Wang,[3] and Cantao Zhuang[3]

Abstract—The little destruction to the deployment site and high repeatability of the Controlled Accurate Seismic Source (CASS) shows its potential for investigating seismic wave velocities in the Earth's crust. However, the difficulty in retrieving impulsive seismic waveforms from the CASS data and identifying the seismic phases substantially prevents its wide applications. For example, identification of the seismic phases and accurate measurement of travel times are essential for resolving the spatial distribution of seismic velocities in the crust. Until now, it still remains a challenging task to estimate the accurate travel times of different seismic phases from the CASS data which features extended wave trains, unlike processing of the waveforms from impulsive events such as earthquakes or explosive sources. In this study, we introduce a time-frequency analysis method to process the CASS data, and try to retrieve the seismic waveforms and identify the major seismic phases traveling through the crust. We adopt the Wigner-Ville Distribution (WVD) approach which has been used in signal detection and parameter estimation for linear frequency modulation (LFM) signals, and proves to feature the best time-frequency convergence capability. The Wigner-Hough transform (WHT) is applied to retrieve the impulsive waveforms from multi-component LFM signals, which comprise seismic phases with different arrival times. We processed the seismic data of the 40-ton CASS in the field experiment around the Xinfengjiang reservoir with the WVD and WHT methods. The results demonstrate that these methods are effective in waveform retrieval and phase identification, especially for high frequency seismic phases such as PmP and SmS with strong amplitudes in large epicenter distance of 80–120 km. Further studies are still needed to improve the accuracy on travel time estimation, so as to further promote applicability of the CASS for and imaging the seismic velocity structure.

Key words: Controlled source, Wigner-Ville distribution, Wigner-Hough transform, seismic waveform, seismic phases.

1. Introduction

The active seismic techniques, such as deep seismic sounding, provide high resolution measurements of the crustal velocity structure. Fruitful results on the seismic velocity structure of the crust have been achieved by classic active seismic techniques with explosion source, which is very important to infer the composition, the tectonic process and evolution of the crust (Christensen and Mooney 1995; Li *et al*. 2006; Nielsen and Thybo 2009). Because of its destructiveness to the environment and difficulties in high repeatability of the explosion source, the Accurately Controlled Routinely Operated Signal System (ACROSS) was developed for investigating crustal seismic velocities (Yamaoka *et al*. 2001; Ikuta *et al*. 2002; Ikuta and Yamaoka 2004; Saiga *et al*. 2006), which demonstrates its potential in imaging the seismic wave velocities of the crust and monitoring its temporal variation. For example, temporal variations of about 2 ms for both P and S waves, together with shear wave anisotropy in a distance of 2.4 km from the source to the receiver, were observed at a site near the rupture fault of the 1995 Kobe earthquake (M7.2) during the 15-month experiment by the ACROSS (Ikuta *et al*. 2002; Ikuta and Yamaoka 2004). Similar powerful low-frequency controlled vibrators had also been tested as a source for active seismology (Alekseev *et al*. 2005; Nielsen and Thybo 2009). Recently, the Controlled Accurate Seismic Source (CASS), which is similar to the ACROSS, has also been developed and tested in the study of shallow and deep crust structures in north China (Wang *et al*. 2009a), in the rupture area of the 2008 Wenchuan earthquake in Sichuan Province (Yang *et al*. 2010) and in the reservoir in South China (Yang *et al*. 2011).

Compared to a chemical explosive source, the CASS is a non-destructive and highly repeatable

[1] State Key Laboratory of Geodesy and Earth's Dynamics, Institute of Geodesy and Geophysics, Chinese Academy of Sciences, Wuhan 430077, China. E-mail: zwli@whigg.ac.cn; sdni@whigg.ac.cn

[2] Key Laboratory of Petroleum Resource Research, Institute of Geology and Geophysics Chinese Academy of Sciences, Beijing 100029, China. E-mail: qyyou0880@mail.iggcas.ac.cn

[3] Institute of Earthquake Science, China Earthquake Administration, Beijing 100036, China.

source, and can continuously work without destroying the surrounding ground. These advantages make it appropriate for investigating the subsurface velocities structure and its possible long-term variations, such as the coseismic and postseismic temporal changes of crustal seismic velocities observed in many studies (Leary *et al*. 1979; Schaff and Richards 2004; Peng and Ben-Zion 2006; Niu *et al*. 2008; Brenguier *et al*. 2008; Wu *et al*. 2009; Xu and Song 2009; Hadziioannou *et al*. 2011; Reasenberg and Aki 1974; Silver *et al*. 2007; Wang *et al*. 2011). The CASS may become an important active source in the investigation of the seismic velocity structure in the shallow and deep crust if the various seismic phases could be identified reliably and their travel times could be measured accurately. However, due to its current limitation in resolution and accuracy as compared to the DSS with explosive source, the CASS could become a helpful complement for the DSS.

The travel times of different seismic phases are the fundamental dataset for imaging the spatial variations of the subsurface structure by using seismological techniques, such as deep seismic sounding and seismic travel time tomography. However, unlike distinct wave pulses usually shown on seismograms from earthquakes and explosive sources, the signals from the CASS data typically feature extended wave trains of oscillation. Retrieval of impulsive seismic waveforms and subsequent reliable identification of the crustal seismic phases (such as Pg, PmP, Sg, and SmS) still remain a substantial challenge, thus further application of the CASS is limited (Yamaoka *et al*. 2001; Ikuta *et al*. 2002; Ikuta and Yamaoka 2004; Saiga *et al*. 2006; Wang *et al*. 2009a; Yang *et al*. 2010, 2011). Thus, retrieval of impulsive waveforms from extended wave trains of the CASS dataset is helpful for identification of the seismic phases and accurate measurement of their arrival time. In this study, we introduced a time-frequency analysis method to retrieve the seismic waveforms from an experiment of a powerful (40-ton) CASS vibrator. Crustal seismic phases (PmP and SmS) are identified on the processed waveforms, and their travel times are also estimated in higher accuracy than previous processing methods such as waveform cross correlation and deconvolution (Wang *et al*. 2009a; Yang *et al*. 2010). Our method attempts to provide another method for the CASS data processing in deep seismic sounding, seismic hazard mapping, seismic station calibration as well as large-structure integrity testing (Alekseev *et al*. 2005). It may also improve the possibility for monitoring the pre- and post-seismic velocity changes if higher accuracy of phase identification can be achieved.

2. Data

2.1. Instrumentation of the Experiment

The seismic data of the CASS are collected from an experiment around the Xinfengjiang reservoir, Guangdong Province of south China during November 2009–January 2010 (Fig. 1). The sinusoidal vibrator of the CASS used in this experiment is the CASS-40 type from the Beijing Gangzhen Mechanical and Technology Co. Ltd. The CASS used in this experiment is similar to that used in the studies of Ikuta *et al*. (2002, 2004), Saiga *et al*. (2006) and Alekseev *et al*. (2005), and has proved successful in north China (Wang *et al*. 2009a) and at the rupture zone of 2008 Wenchuan earthquake (M_w 7.9) (Yang *et al*. 2010). The CASS generates a sinusoidal force in vertical direction by rotating a pair of eccentric masses in opposite directions (shown in Fig. 2) (Liao *et al*. 2003; Wang *et al*. 2009a). The pair of eccentric masses is driven by a pair of 55 KW servo motors with a phase feedback controller. The rotation of the servo motors is accurately controlled with synchronization by the GPS clock. The phase precision of the rotation of the eccentric mass pair is always better than 0.3°. The CASS used in this experiment sweeps in the frequency bands between 5 and 10 Hz, and its effectiveness and reliability have been proven in the utilization in north China (Wang *et al*. 2009a). In total, 81 temporary EDAS-BS60 broadband (flat response in the band of 60 s-80 Hz), three-component seismographs are deployed to record the ground motions excited by CASS (Fig. 1), with epicentral distances (the distance between the seismic stations and the CASS vibrator) from 5 to 200 km. One seismograph is deployed very close to the CASS sources (with distances about 30–50 m) to record near field vibrations, which will be used to extract the source time function. A sampling rate of 200 samples-per-second (sps) are used for all seismic stations.

2.2. *Description of the Experiment*

The CASS was deployed at four sites around the Xinfengjiang reservoir, Guangdong Province, south China (Fig. 1). Since Xinfengjiang reservoir began filling with water in 1959, seismicity has increased rapidly in the reservoir area, producing one of the largest induced earthquake of M6.1 on 19 March 1962 (YANG *et al*. 2011). In order to investigate the crustal velocity structure and its possible relations to the reservoir induced earthquakes, a deep seismic wide-angle reflection/refraction profile with two explosion sources, 81 temporary seismic stations, together with the CASS vibrators at four sites were deployed around the Xinfengjiang reservoir (YANG *et al*. 2011). For the CASS vibrators, rather than using the single frequency signals as adopted in the previous studies (IKUTA *et al*. 2002; IKUTA and YAMAOKA 2004), the linear frequency modulation (LFM) signals were excited by the CASS vibrator-1 (Yingde source), vibrator-3 (Longchuan source) and vibrator-4 (Zengcheng source) (Fig. 1). For the CASS vibrator-2 (Heyuan source), a sinusoidal frequency modulation scheme was adopted for exciting seismic signals, and is not included in this study. The excitation of one cycle lasts 1 h. As shown in Fig. 3a, the CASS works for the first 3,000 s (excitation stage) with five small cycles with duration of 600 s, and is at rest in the last 600 s (rest stage) for each hour. In the 600 s of each small cycle, the LFM signals are sweeping linearly from 5 to 10 Hz in the first 300 s and 10 to 5 Hz in the last 300 s, then totally repeat five times (as shown in Fig. 3b). The waveforms and spectrograms of the 1-h LFM signals recorded at the CASS vibrator-1 (Yingde source) are

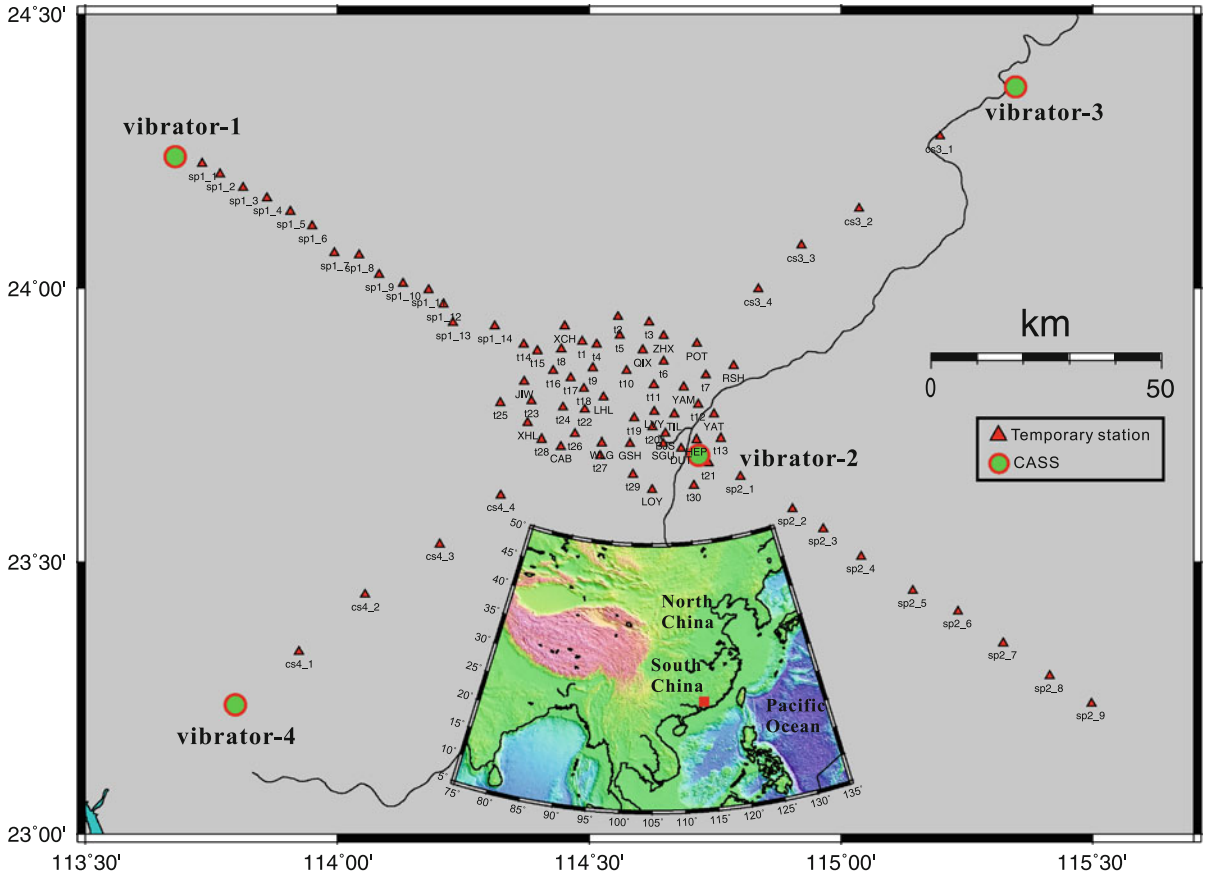

Figure 1
Four CASS vibrators (*green circles*) and 81 temporary seismic stations (*red triangles*) deployed around the Xinfengjiang reservoir. The *red square* in the *inset* map shows the location of this experiment

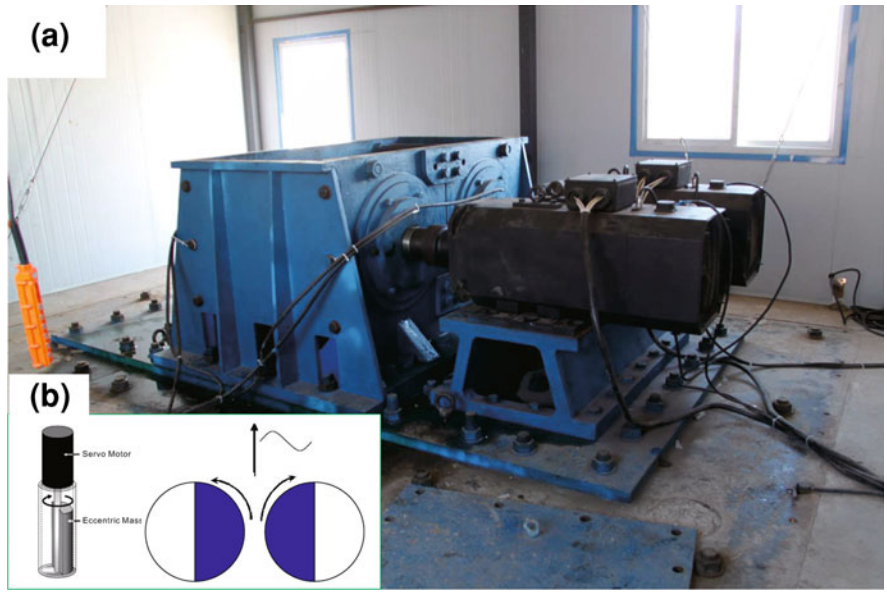

Figure 2
a The equipment of a CASS vibrator. **b** The seismic signal excitation mechanism of the CASS. A pair of eccentric masses are driven by a pair of 55 KW servo motors with phase feedback controller and rotating in the opposite directions, which generate a sinusoidal vertical force up to 40 tons in the vertical direction

displayed in Fig. 3. In the last 600 s in each hour, the CASS is at rest and only background noise is recorded in the seismic waveforms, making it convenient to compare the signals and the noises in the two stages. The CASS at each location worked for 37 h during the experiment, and most of the experiments were conducted at mid-night due to the relatively lower background noise.

3. Method and Data Analysis

3.1. Method

In previous studies of rotational vibrators, three methods of transfer function, waveform correlation and deconvolution were adopted to retrieve waveforms and measure travel times of seismic waves (IKUTA *et al*. 2002; IKUTA and YAMAOKA 2004; ALEKSEEV *et al*. 2005; SAIGA *et al*. 2006; WANG *et al*. 2009a; YANG *et al*. 2010). However, it's difficult to determine spatial distribution of temporal variation of velocities because no distinct seismic phases of impulsive waves can be identified. Seismic waveforms from the approaches of correlation and deconvolution are also characterized by relative low time resolutions, which is partially due to the narrow frequency band of the excited signals (5–10 Hz). Thus, the well defined seismic phases on seismograms from earthquakes and chemical explosions, such as Pg, PmP, Sg, and SmS, cannot be clearly identified in the processed waveform from CASS experiments. Since the crustal seismic phases are essential for monitoring the velocity variations and imaging the crustal structures, it's necessary to retrieve the impulsive seismic waveforms, identify the crustal seismic phases and interpret their travel times from the CASS data.

It would be ideal if a seismic source excites a delta-function source time function (very short pulse). But for a strong enough impulsive excitation, the deployment site will be damaged and repeatability is difficult to achieve. Instead, the CASS spreads excitation energy in time (up to 300 s) and frequency (5–10 Hz); therefore, it will not cause substantial damage to the deployment site. However, the challenge is to reconstruct impulsive signals from the extended wave trains. The CASS excites the LFM signals in two stages. In the first stage, the frequency increases from 5 to 10 Hz and in the second stage, the frequency decreases from 10 to 5 Hz (Fig. 3b). The LFM signal

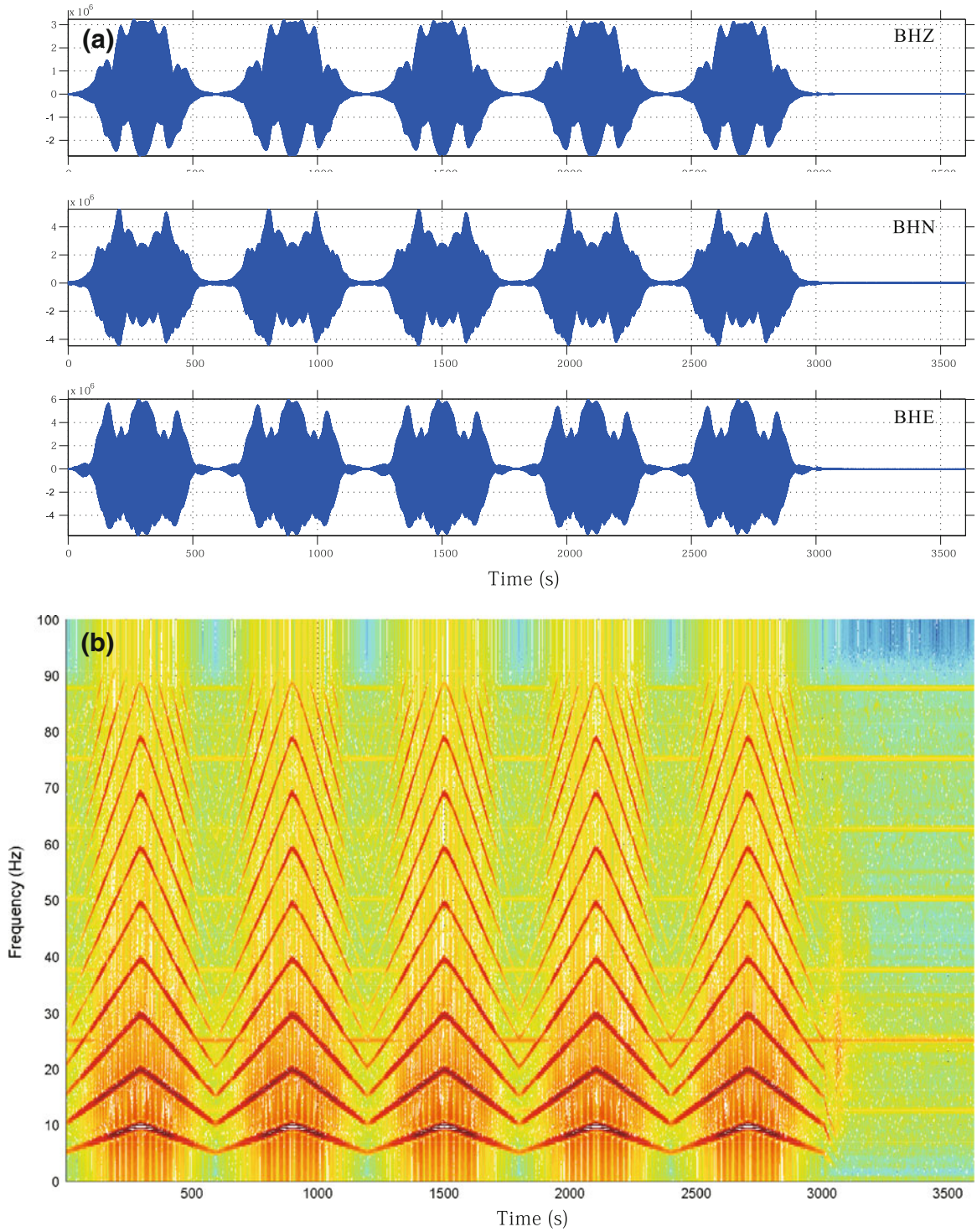

Figure 3

a One-hour raw 3-component seismic data recorded by the seismic stations very close to the CASS vibrator-3. **b** The spectrograms of the vertical component data from the CASS vibrator-3 analyzed with a Short-Time Fourier Transform (STFT) algorithm. The linear frequency modulation (LFM) signals vary between 5 and 10 Hz in each 300 s time window, which are very clear in the spectrograms. In addition, the multiple harmonic LFM signals are also very clear

has been widely used in the RADAR, SONAR and communication systems (Barbarossa 1995). Time-frequency analysis algorithms, such as Short-Time Fourier Transform (STFT), Wavelet Transform (WT) and Wigner-Ville Distribution (WVD), have proved effective for processing the LFM signal. However, the width of the windowing function of STFT is fixed, and the time window of WT is also varying with frequency, which could compromise the resolution in both time and frequency domains for signal detection and parameter estimation (Haimovich *et al.* 1994). Whereas the WVD algorithm has the best time-frequency concentration capability for the LFM signals (Rao and Taylor 1990), which makes it especially appropriate for processing the seismic signals in this study. The WVD of signal $x(t)$ can be defined as:

$$\mathrm{WVD}_x(t,f)=\frac{1}{2\pi}\int_{-\infty}^{+\infty}x\left(t+\frac{\tau}{2}\right)x*\left(t-\frac{\tau}{2}\right)e^{-j2\pi f\tau}d\tau \tag{1}$$

The time-frequency convergence capability of the WVD for the LFM signal is the best (Rao and Taylor 1990). But when processing the multi-component signals such as the CASS data., the cross-term will contaminate the resolution in both time and frequency domains because the WVD is a bilinear function of the signal (Selin and William 2005).

As the WVD can desirably concentrate the LFM signals in the time-frequency plane, the Hough transform (HT) can be applied with the WVD to suppress the cross-time interference, which is better than the WVD in detecting the multi-component LFM signals (Choi and Williams 1988; Barbarossa 1995). The Wigner-Hough transform (WHT) is defined as:

$$\mathrm{WH}_x(f,\beta)=\int_{-\infty}^{+\infty}\int_{T}x(t+\frac{\tau}{2})x^*(t-\frac{\tau}{2})e^{-j2\pi(f+\beta t)\tau}dtd\tau \tag{2}$$

3.2. Seismic Data of the CASS

In order to improve the SNR and reduce computation cost, the original CASS data are pre-processed, including the band pass filtering and down-sampling. The original data are band pass filtered between 5 and 10 Hz since the signals excited by the CASS only contain source energies between 5 and 10 Hz, and down-sampled into 20 sps from 200 sps. The WHT is applied on each 300 s segment of CASS data with the frequency increasing (5–10 Hz) or decreasing (10–5 Hz) signals (as shown in Figs. 3, 4). Theoretically, the energy excited by the CASS increases with the frequency due to the mechanical implementation scheme. Actually, the amplitudes of the observed waveform from the CASS vibrator-1 are not monotonously increasing with the frequency (Fig. 3a). One possible reason could be attributed to the site response beneath the CASS. In order to enhance the mechanical coupling with ground, CASS is installed on the top of soil, that is, at site of unconsolidated sediments. The disadvantage of installing the instrument on sediment is that the soils may present frequency dependent amplification of the ground motion, thus leading to some distortion to the input source signals.

Figure 4 shows the raw seismic data and its spectrograms of processed three-component data recorded at station *sp1_1*, and the source is the CASS vibrator-1. The spectrograms of the waveforms are analyzed with a STFT algorithm, and its time-frequency concentration capability is not as good as the WVD. However, given its small epicentral distance ($\sim$5.6 km) to the CASS, the LFM signals at the source and station *sp1_1* are still very similar and clear (Fig. 4b). Figure 5 shows the spectrograms of the down-sampled vertical component data recorded at the source site of CASS vibrator-1 and station *sp1_1*, which are analyzed using the WVD algorithm. Compared to the spectrograms from the STFT algorithm displayed in Figs. 3b and 4b, the LFM signals from the WVD algorithm are much clearer (Fig. 5). It suggests the outstanding time-frequency convergence capability of the WVD for the LFM signal (Rao and Taylor 1990). When the epicentral distance becomes larger, the LFM signals become unclear on raw spectrograms, but can still be retrieved using the WHT method.

4. Results and Discussion

With the WHT algorithm, we processed the seismic data excited by the three CASS vibrators with

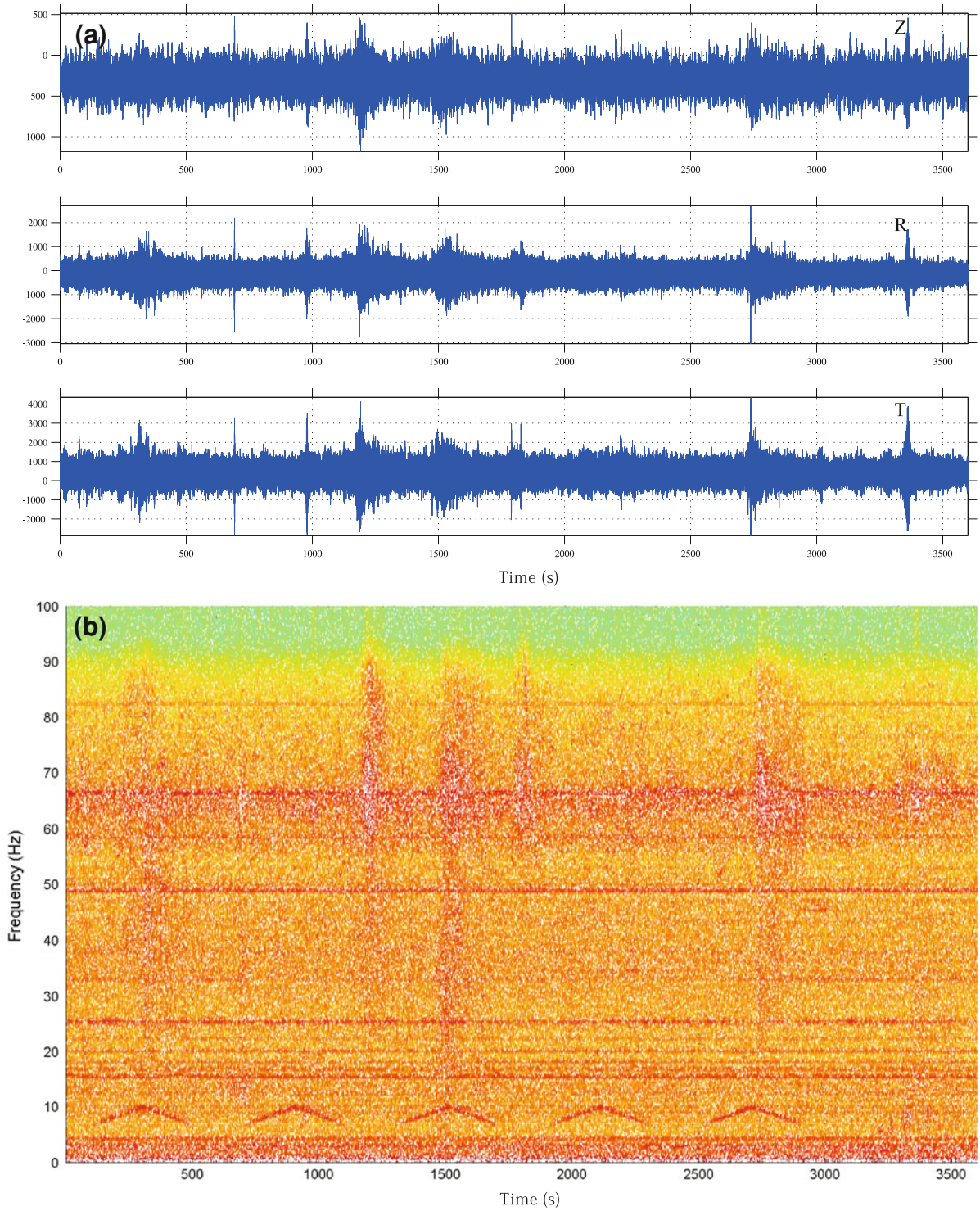

Figure 4

a One-hour raw 3-component seismic data recorded by the seismic station of sp1_1 from the CASS vibrator-1. **b** The spectrograms of the vertical component analyzed by using a STFT algorithm. The epicentral distance from the sp1_1 station to the CASS vibrator-1 is about 5.6 km. The LFM signals are also very clear in the spectrograms

LFM signals (vibrator-1, vibrator-3 and vibrator-4). The waveforms recorded at the source site and remote stations are all processed. In the processing, seismic waveforms are retrieved from each 300-s-long data with 5–10 and 10–5 Hz LFM signals, and then stacked to improve the SNR. Waveforms for the frequency increasing stage (5–10 Hz) and decreasing stage (10–5 Hz) are retrieved respectively, as the WHT algorithm only works for a window of data with one linear trend of frequency modulation. Figure 6 shows the seismic waveforms retrieved from the vertical component data recorded at the source site of the CASS vibrator-1, vibrator-3 and vibrator-4. As shown in the upper row of Fig. 6, the waveforms retrieved from each 300-s-long data are highly similar, which can also match each other very well, indicating the excellent repeatability and the high accuracy of the waveform retrieval of the CASS data (Note that the amplitudes of these waveforms are not normalized). For the noise data in the last 600 s of each hour, no obvious signals emerge in the retrieved waveform (Fig. 6), which also proves that the waveforms retrieved from 0 to 3,000 s in each hour are excited by the CASS. Since there are five cycles of excitation for each hour, for the whole 37 h of experiment, we obtain 175 samples of waveforms for

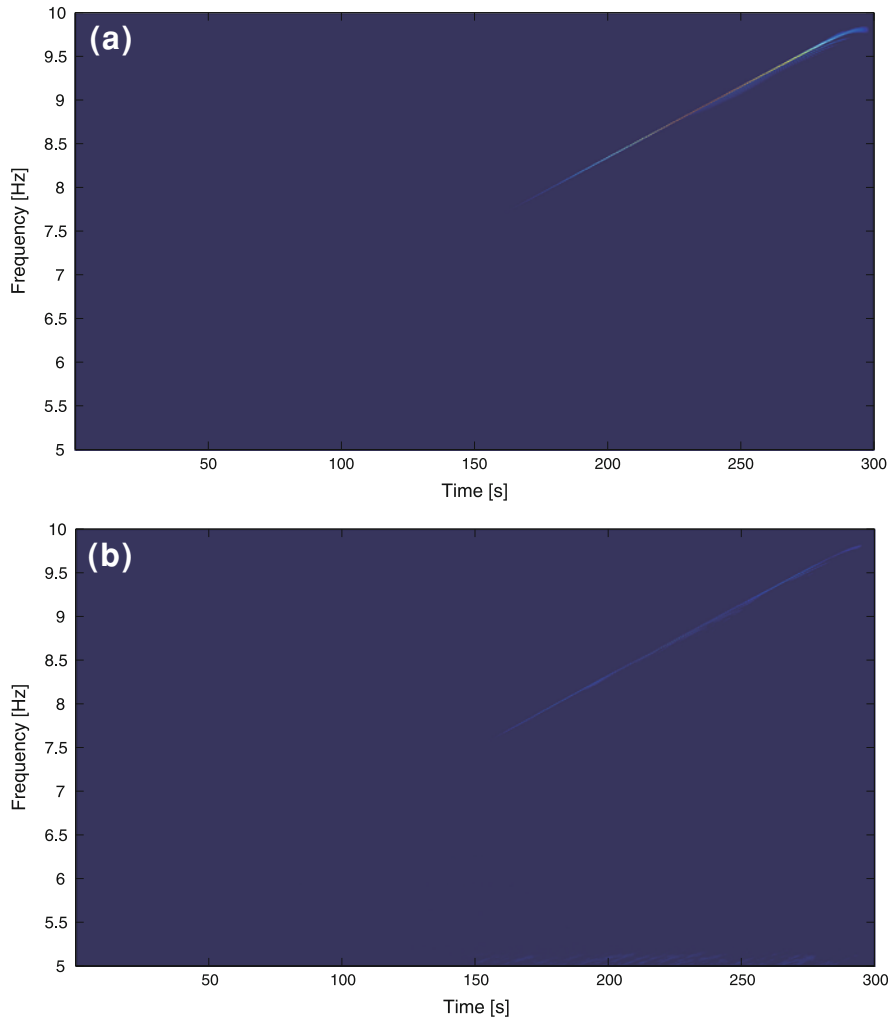

Figure 5
The spectrograms of 300-s length vertical component seismic data analyzed with the WVD algorithm. **a** The data is recorded near the CASS vibrator-1; **b** the data is recorded at the station sp1_1. Note that the LFM signals are much clearer than the spectrograms derived from the STFT algorithm

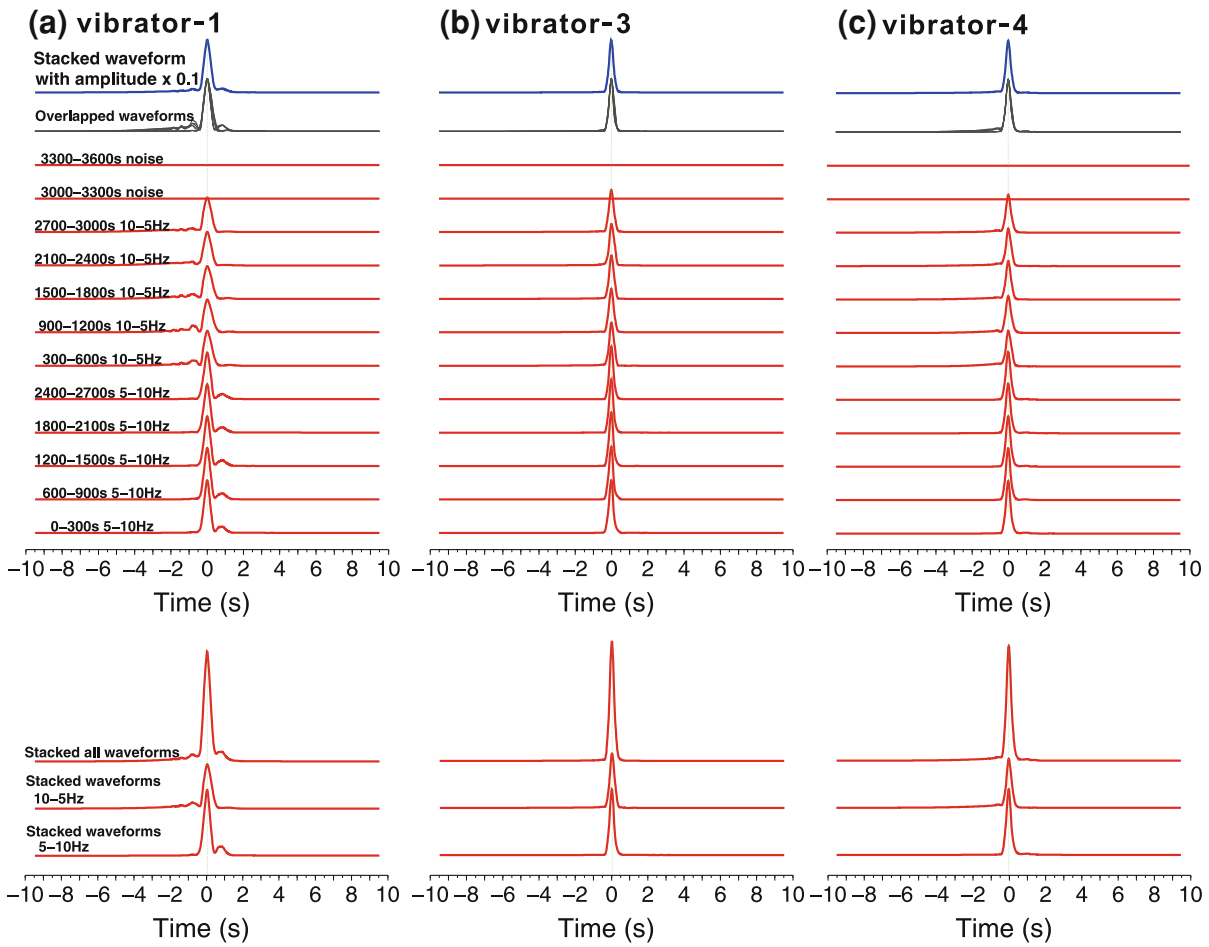

Figure 6

The waveforms retrieved from the 1-h vertical component data (*upper*) and stacked waveforms (*lower*) from the CASS **a** vibrator-1, **b** vibrator-3, and **c** vibrator-4. The time period has been labeled on the *left side* of retrieved waveforms in Fig. 6a, which is the same for Fig. 6b, c. No obvious signals appear in the time period of 3,000–3,600 s, when CASS is at rest. The retrieved waveforms can overlap each other very well, suggesting the high repeatability of the signal excitation of the CASS. Note that the amplitude of waveforms are not normalized

the 5–10 Hz stage and the 10–5 Hz LFM stage. High quality waveforms are stacked to form the waveform to be used as source time function for the CASS vibrator-1, and the zero time is defined to be aligned with the highest amplitude. The lower row of Fig. 6 shows the source time function for 5–10 and 10–5 Hz LFM signals after stacking, as well as the final wavelets (sum of source time function for both 5–10 and 10–5 Hz stage) for the CASS vibrator-1, vibrator-3 and vibrator-4. All the retrieved waveforms from the same vibrator are extremely similar.

In order to quantify the repeatability of each CASS vibrator, we calculated cross-correlation coefficients of all waveform pairs retrieved from different time windows. Figure 7 shows the distributions of all the cross-correlation coefficients for the CASS vibrator-1, vibrator-2 and vibrator-4. For the waveform pairs of the CASS vibrator-1 (Fig. 7a), more than 32 % of cross-correlation coefficients for 5–10 Hz LFM signals and more than 21 % for 10–5 Hz LFM signals are greater than 0.998. For the CASS vibrator-3 (Fig. 7b), the percentages of the cross-correlation coefficients increase to more than 36 % for 5–10 Hz and more than 34 % for 10–5 Hz LFM signals greater than 0.998. The CASS vibrator-4 (Fig. 7c) has the greatest percentages of cross-correlation coefficients higher than 0.998. The percentages are more than 60 % for both 5–10 and 10–5 Hz LFM

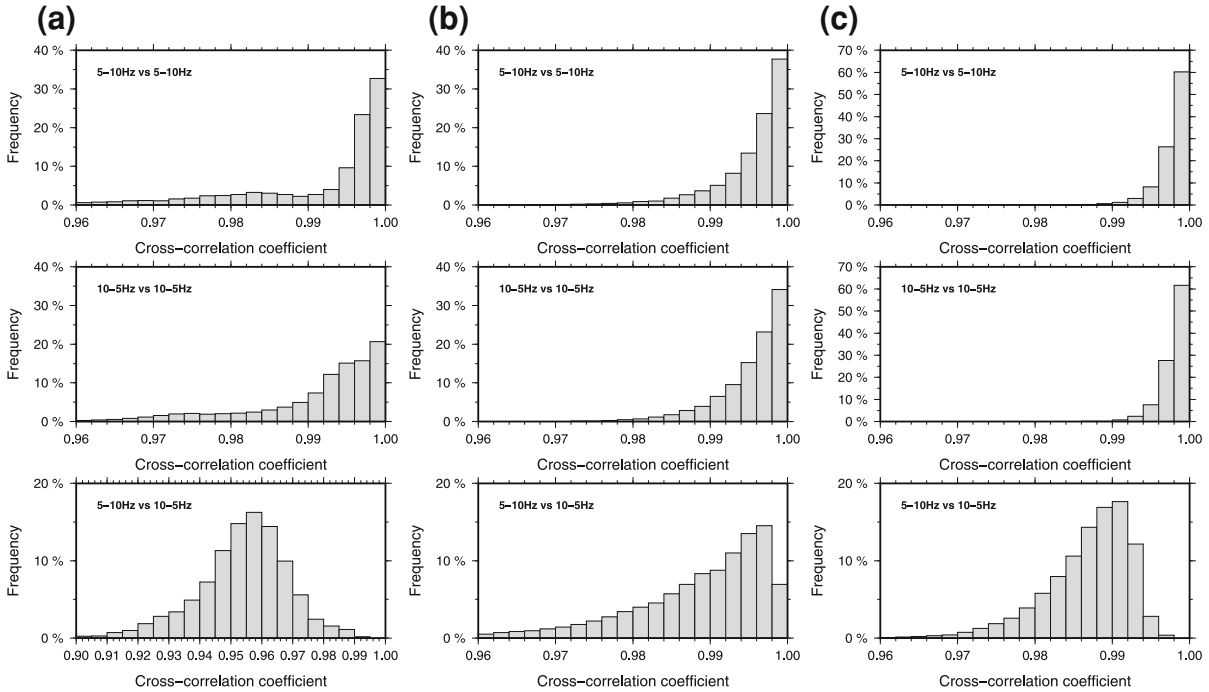

Figure 7
Distributions of the cross-correlation coefficients of the all retrieved waveform pairs for the CASS vibrator-1 (**a**), vibrator-2 (**b**) and vibrator-4 (**c**). The *upper row* shows the distributions of cross-correlation coefficients between waveforms with 5–10 Hz LFM signals. The *middle row* shows the same figures as the *upper row* but for waveforms with 10–5 Hz LFM signals. The *lower row* shows the distributions of cross-correlation coefficients between waveforms combined with both 5–10 and 10–5 Hz LFM signals. High correlations between the waveforms indicate the excellent repeatability of the CASS vibrator

signals. The high percentages of cross-correlation coefficients higher than 0.998 suggest the equivalent or better repeatability compared to the repeated earthquakes (Schaff and Richards 2004; Wang *et al.* 2009b) and air gun (Chen and Li 2007a; Chen *et al.* 2007b; Wang *et al.* 2010).

Noticeable differences between the retrieved waveforms for the 5–10 and 10–5 Hz LFM signals are observed, especially for the CASS vibrator-1. As shown in Fig. 6a, the side lobes with smaller amplitudes appear at $\sim$1 s after the peak of the waveform for the 5–10 Hz LFM signals, while they are at $\sim$1 s before the peak for the 10–5 Hz LFM signals. The systematic differences could probably be induced by the CASS itself or the site response to different frequencies. In order to determine whether the CASS itself induces the sidelobes for different LFM signals or not, we also compared the retrieved waveforms for the CASS vibrator-3 and vibrator-4, but no obvious sidelobes are found. The sidelobes of the CASS vibrator-4 are a litter stronger than the CASS vibrator-3 but much weaker than the CASS vibrator-1. Thus, we infer that the sidelobes appearing in the retrieved waveforms are possibly not induced by the CASS itself. The site response, including the velocity structures of the sediments beneath the CASS vibrator and/or the seismic station, may induce the resonance of seismic wave at some frequency (Ni *et al.* 1997). These could be the possible sources of the sidelobes in the retrieved waveforms.

In order to check how far the LFM signals can propagate through the crust from the 40-ton CASS, we also processed the seismic data recorded at remote stations far away from the CASS vibrators. The epicentral distances are from $\sim$5 to $\sim$140 km. Figure 8 shows record sections of the retrieved waveforms with high SNR recorded at epicenter distances from $\sim$5 to $\sim$110 km for the CASS vibrator-1 (Fig. 8a), vibrator-3 (Fig. 8b) and vibrator-4 (Fig. 8c). Since the retrieved waveforms are aligned with respect to

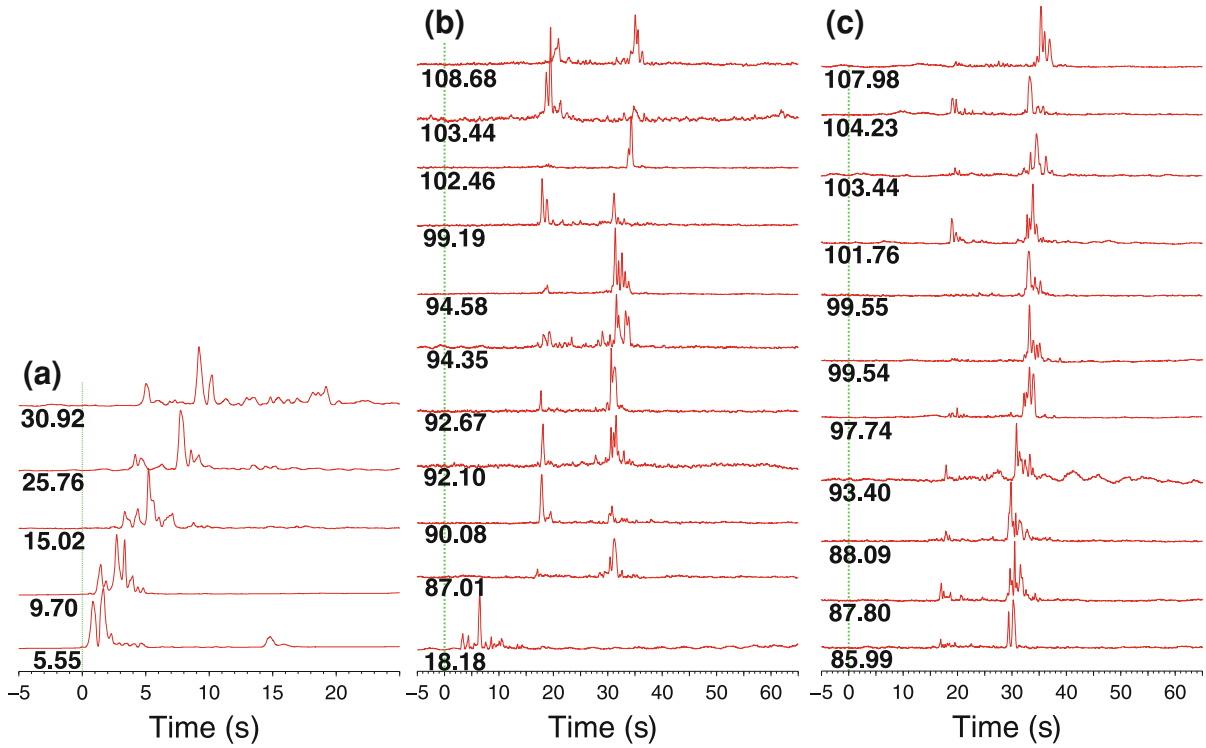

Figure 8
The retrieved waveforms with the WHT algorithm for data of the CASS vibrator-1 (**a**) vibrator-2 (**b**) and vibrator-3 (**c**). Note that the epicenter distance (km) from the seismic station to the source is labeled on the *left* below each waveform

the peak of the source time function, the arrivals of the seismic phases are then defined with their peaks rather than the onset time of the seismic phases in traditional observations for earthquake and explosion sources. For distances less than 40 km, the first and second peaks could possibly represent the arrivals of the direct Pg and Sg, respectively, inferred from the apparent velocities around 5–6 km/s for the first peaks and 2.6–3 km/s for the second peaks. Particularly for the waveform at a distance of 5.55 km (Fig. 8a), a peak with $\sim$15 s delay appears with apparent velocity of $\sim$0.37 km/s. We interpret it as the Rayleigh wave induced by the ACCORSS vibrator. Similar characteristics are also shown both for the CASS vibrator-3 (Fig. 8b) and vibrator-4 (Fig. 8c), except the Rayleigh wave with high frequency (5–10 Hz) has been rapidly attenuated with the increasing of epicenter distance. Compared to the retrieved waveforms by the cross-correlation algorithm, obvious oscillations appear in their results, which is hard for identification of the seismic phases and accurate measurement of their arrival times.

In order to identify the seismic phases in the waveform and measure their travel times for our observations, we firstly calculated synthetic waveforms from 1-D models with the frequency-wave number integral method (Zhu and Rivera 2002) (Fig. 9). A four-layer 1-D model of south China (Fig. 9b) was proposed by Li *et al.* (2006). As we only want to compare the direct waves (Pg and Sg) and the reflected waves (PmP and SmS) from the Moho discontinuities; therefore, we propose another 1-D model, which is basically a smoothed version of Li *et al.* (2006) (Fig. 9d). The synthetic waveforms (Fig. 9c) from this model show similar characteristics to the observed seismic record sections for the explosion experiment, suggesting that this 1-D model is proper for performing forward ray tracing and implementing the comparison with the controlled source profiles. The deep seismic sounding profiles are not in the same location as in our controlled source observation, which could be the reason why their four-layer 1-D model does not work well in this area (Li *et al.* 2006).

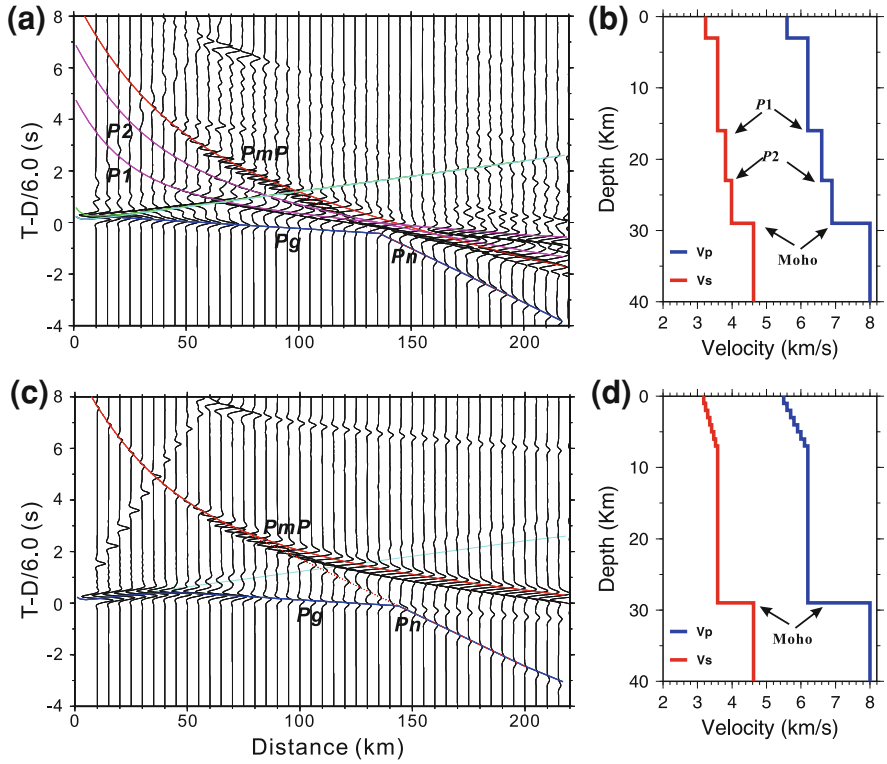

Figure 9
Synthetic P-waves from two 1-D models. The four-layer model (**b**) is derived from Li *et al*. (2006), and the smoothed 1-D model (**d**) is used to analyze our observation

We plot the retrieved waveforms with reduced velocity of 8.0 km/s for P-waves (Fig. 10a) and 4.6 km/s for S-waves (Fig. 10b). In order to implement the comparison conveniently, the waveforms are normalized to 1. Synthetic arrival times of Pg, PmP, Sg and SmS are also overlaid with the seismograms. The 1-D velocity model shown in Fig. 9d is adopted in the travel time computation. As expected, the delay times of the first and second major peaks are consistent with the first arrival of Pg and Sg within ~40 km epicentral distance in all cases. For epicentral distances up to 80–120 km, the first and second major peaks are consistent with the arrival time of PmP (Fig. 11a) and SmS (Fig. 11b), respectively. In Fig. 10b, the predicted arrival times of SmS also fit well on the waveform peaks at 55–65 km epicentral distances for vibrator-3. The good consistency between the theoretical arrival times of PmP and SmS and high SNR of the waveforms are quite clear in the Fig. 11 when the waveform profiles are zoomed and compared to the synthetic waveform with single force source in the epicentral distances between 80 and 120 km. Bakun *et al*. (1984) and Hutton *et al*. (1987) observed systematic strong amplitudes in the seismic waveforms at epicentral distances from 60 to 125 km and attributed these energy with strong amplitudes to the SmS. If the crustal structure is appropriate, the SmS will be fully reflected in the post-critical distance and become much stronger than the direct S wave (Mori and Helmberger 1996; Liu and Tsai 2009; Luo *et al*. 2010). In addition, the high frequency Rayleigh wave excited by the 5–10 Hz LFM signals should rapidly attenuate with epicentral distance. Therefore, we infer that the maximum peaks are most probably the SmS wave rather than the Sg wave or Rayleigh wave. Identification of the Moho-reflected waves for PmP or SmS is crucial for studying the velocity structure and its temporal variation of lower crustal structures, which are believed to be more ductile and deformable. For example, postseismic processes including afterslip and relaxation after large earthquakes (>M7)

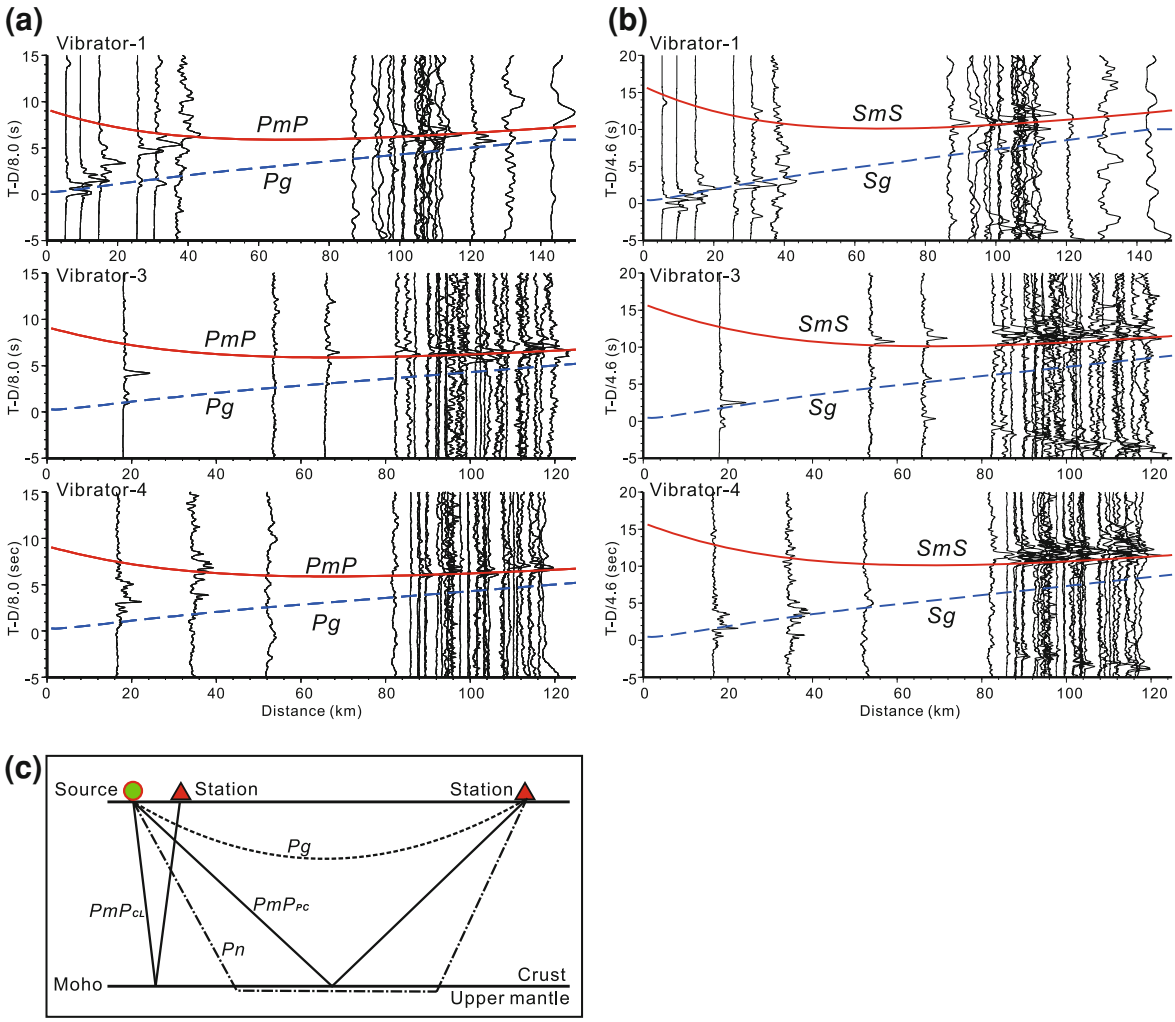

Figure 10

All retrieved P-waves (**a**) and S-waves (**b**) from the CASS vibrator-1, vibrator-3 and vibrator-4. Reduced velocities are 8.0 km/s for P-waves and 4.6 km/s for S-waves. Theoretical arrival time of Pg, PmP, Sg and SmS from 1-D model are all *plotted* within this map. (**c**) Scheme of seismic phases traveling through the crust. PmPcl is the PmP phase at close distance far from the post critical distance, whereas PmPpc is the PmP phase at overcritical distances

typically occur in middle and lower crust, and their time scale is in the range of months up to years (Diao *et al*. 2011).

Another interesting characteristic is that the amplitudes of the peaks on the retrieved waveforms rapidly varies, even for two stations at very close epicentral distances. Usually the peaks represent the energy of different seismic phases, the rapid variations of the amplitude of the peaks may be possibly attributed to the very different site response beneath the seismic stations or rapid lateral variation in deep crust or Moho topography for the case of Moho-reflected phases of PmP and SmS. For example, the thickness and the S-wave velocity of sediments will largely alter the amplitudes of certain seismic phases at different frequencies (Ni *et al*. 1997), which will probably complicate the analysis of the retrieved high frequency waveforms. Further efforts are still needed to estimate the accurate absolute travel times of different seismic phases. However, clear waveforms have already been retrieved from the CASS as far as $\sim$140 km distance by the WVD and WHT methods. The high repeatability of the CASS has also been suggested by our results. If much clearer seismic

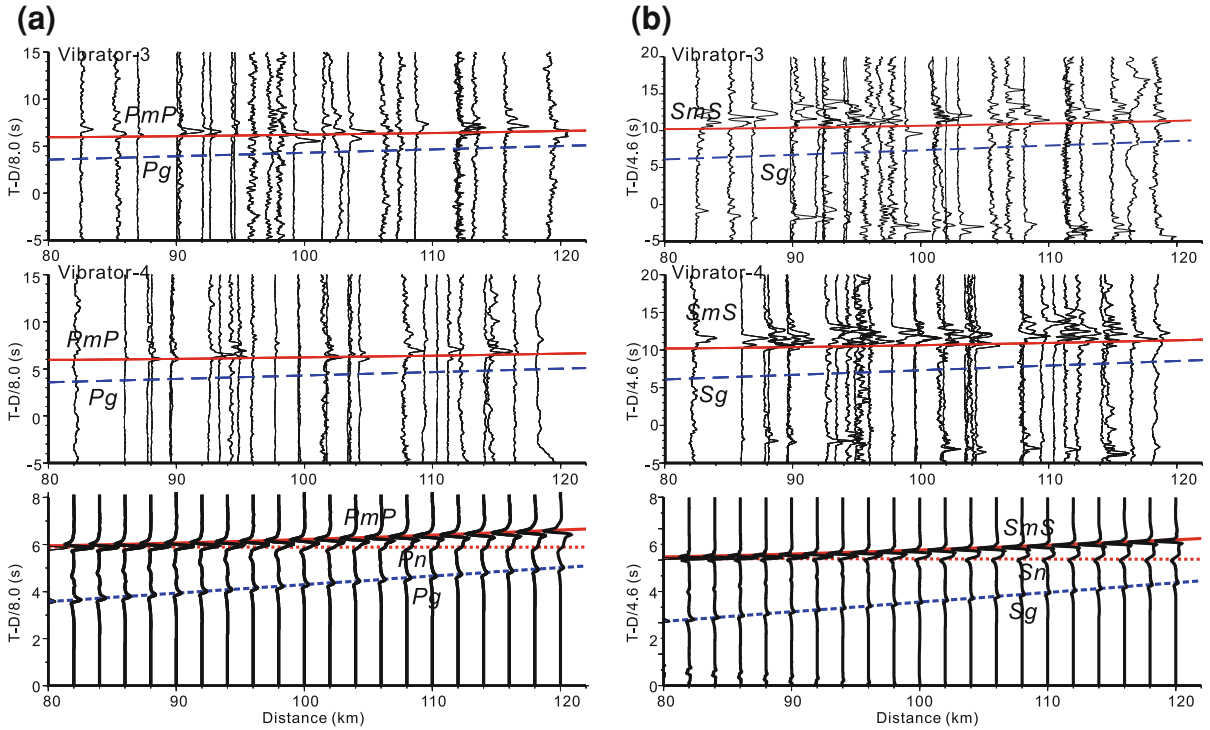

Figure 11
Recorded sections of P-waves (**a**) and S-waves (**b**) for vibrator-3 (*upper row*) and vibrator-4 (*middle row*) zoomed in the epicentral distances between 80 and 120 km. The *bottom row* shows the synthetic P- and S-waves calculated from the 1-D model. Note that the amplitude of PmP (SmS) is much larger than Pg (Sg) in the synthetic waveforms

phases and more accurate travel time could be achieved from the CASS data, by using the travel time difference between two retrieved waveforms from the CASS data in different period, it could be possible to monitor temporal variations of the seismic velocities beneath the reservoir, the fault zone with active seismicity and even the whole crust. It could also be very helpful to imaging the spatial variation of crustal velocities.

However, there are some issues not taken into account in this study such as possible wave dispersion and attenuation for different frequencies. Theoretically, higher frequency signals attenuate more with larger distances, therefore the signals recorded at a remote site could show different spectrum as the source time function. Moreover, waves could propagate at different speed for different frequency (i.e., dispersion), which also may complicate our study. For simplicity, we assume both effects of dispersion and attenuation are not significant, as demonstrated by the relatively stable waveforms recovered for different distances.

5. Conclusion

The CASS may become a useful source for investigating seismic wave velocity structure of the crust in the future. However, the difficulty of retrieving the impulsive waveforms from the CASS data, identifying the seismic phases and measuring their travel times greatly prevent its wide applications. In this study, we introduced the time-frequency analysis algorithms of WVD and WHT into the waveform retrieval from the CASS data. The WVD algorithm has the best time-frequency concentration capability for the LFM signals. The WHT algorithm is helpful to suppress the cross-time interference in the signal detection and parameter estimation for the multi-component LFM signals. Application of the WVD and WHT algorithms are also conducted on the 40-ton CASS data from the experiment in the Xinfengjiang reservoir. The results suggest that it is effective in the waveform retrieval, seismic phase identification and travel time measurement, especially

for PmP and SmS phases with strong amplitude in some epicenter distances. The seismic source with high repeatability, such as the CASS, is indispensible for monitoring temporal changes and imaging the spatial variations of the subsurface structure. Our method provides a feasible way to process the CASS data and advance its application in monitoring the crustal processes. However, in order to meet the requirement on the accuracy for imaging the seismic wave velocity structure and its temporal changes of the crust with CASS data, further studies are still needed to improve the accuracy of phase identification and travel time estimation.

Acknowledgments

We would like to thank the Editor, Dr. Elena Kozlovskaya, Dr. Mariusz Majdanski and an anonymous reviewer for their valuable comments, which greatly improved the manuscript. This work was supported by China Earthquake Administration fund (Grant No. 200808068), NSFC (Grant No. 41074032) and special fund from the State Key Laboratory of Geodesy and Earth's Dynamics.

References

Alekseev, A.S., Chichinin, I.S. and Korneev, V.A., 2005. *Powerful low-frequency vibrators for active seismology*. Bull. Seismol. Soc. Am., *95*, 1–17.

Bakun, W.H. and Joyner, W.B., 1984. *The M_L scale in central California*. Bull. Seismol. Soc. Am., *74*, 1827–1843.

Barbarossa, S., 1995. *Analysis of multicomponent LFM signals by a combined Wigner-Rough transform*. IEEE Signal, *43*, 1511–1515.

Brenguier, F., Campillo, M., Hadziioannou, C., Shapiro, N.M., Nadeau, R.M. and Larose, E., 2008. *Postseismic relaxation along the San Andreas Fault at Parkfield from continuous seismological observations*, Science, *321*, 1478–1481.

Chen, Y. and Li, Y.J., 2007a. Seismic wave radar research: using active source to detect continental crust structure. J. Univer. Sci. and Tech. of China, *37*, 813–819.

Chen, Y., Zhang, X.K., Qiu, X.L., Ge, H.K., Liu, B.J. and Wang, B.S., 2007b. *A new way to generate seismic waves for continental crustal exploration*. Chinese Sci. Bull., *52*, 1317–1321.

Choi, H. and Williams, W.J., 1988. *Improved time-frequency representation of multicomponent signals using exponential kernels*. IEEE Trans on SP, *37*, 862–871.

Christensen, N.I. and Mooney, W.D., 1995. Seismic velocity structure and composition of the continental crust: A global view. J. Geophys. Res., 100, B7, 9761–9788.

Diao, F., Xiong, X. and Wang, R., 2011. Mechanisms of transient postseismic deformation following the 2001 Mw 7.8 Kunlun (China) Earthquake.. Pure App.Geophys., *168*, 767–779.

Hadziioannou, C., Larose, E., Baig, A., Roux, P. and Campillo, M., 2011. *Improving temporal resolution in ambient noise monitoring of seismic wave speed*. J. Geophys. Res., *116*, B07304.

Haimovich, A.M., Peckham, C. and Teti, J.G., 1994. SAR imagery of moving targets: Application of time-frequency distributions for estimating motion parameters. In: Proc 1994 SPIE's International Symposium on Aerospace and Sensing, *2238*, 238–247.

Hutton, L.K. and Boore, D.M., 1987. *The M_L scale in southern California*. Bull. Seismol. Soc. Am., *77*, 2074–2094.

Ikuta, R., Yamaoka, K., Miyakawa, K., Kunitomo, T. and Kumazawa, M., 2002. *Continuous monitoring of propagation velocity of seismic wave using ACROSS*. Geophys. Res. Lett., *29*, 1627.

Ikuta, R. and Yamaoka, K., 2004. *Temporal variation in the shear wave anisotropy detected using the Accurately Controlled Routinely Operated Signal System* (*ACROSS*). J. Geophys. Res., *109*, B09305.

Leary, P.C., Malin, P.E., Phinny, R.A., Brocher, T. and Von-Colln, R., 1979. *Systematic monitoring of millisecond traveltime variations near Palmdale, California*. J. Geophys. Res., *84*, 659–666.

Li, S.L., Mooney, W.D. and Fan, J.C., 2006. *Crustal structure of mainland China from deep seismic sounding data*. Tectonophysics, *420*, 239–252.

Liao, C.W., Zhuang, C.T. and Liang, H.S., 2003. *Initial experimental result of Accurately Controlled Routinely Operated Signal System* (ACROSS). Earthq. Res. in China, *19*, 89–96.

Liu, K. S. and Tsai, Y. B., 2009. *Large effects of Moho reflections* (*SmS*) *on peak ground motion in Northwestern Taiwan*. Bull. Seismol. Soc. Am., *99*, 255–267.

Luo, Y., Ni, S.D. and Chen, Y., 2010. *A case study on the effect of post-critical SmS on ground motion in Yingjiang*, *Yunnan Province*, *China*. Earthq. Res. in China., *26*, 131–141.

Mori, J. and Helmberger, D.V., 1996. *Large-amplitude Moho reflection* (*SmS*) *from Landers aftershocks, southern California*, Bull. Seismol. Soc. Am., *86*, 1845–1852.

Ni, S.D., Siddharthan, R.V. and Anderson, J.G., 1997. *Characteristics of nonlinear response of deep saturated solid deposits*. Bull. Seismol. Soc. Am., *87*, 342–355.

Nielsen, C. and Thybo, H., 2009. *Lower crustal intrusions beneath the southern Baikal Rift Zone*: *Evidence from full-waveform modelling of wide-angle seismic data*. Tectonophysics, *470*, 298–318.

Niu, F.L., Silver, P.G., Thomas, D.M., Cheng, X. and Majer, E.L., 2008. *Preseismic velocity changes observed from active source monitoring at the Parkfield SAFOD drill site*. Nature, *454*, 204–208.

Peng, Z. and Ben-Zion, Y., 2006. *Temporal changes of shallow seismic velocity around the Karadere-Duzce branch of the North anatolian fault and strong ground motion*. Pure Appl. Geophys., *163*, 567–599.

Rao, R. and Taylor, F.J., 1990. *Estimation of instantaneous frequency using the discrete Wigner distribution*. Electr. Lett., *26*, 246–248.

Reasenberg, P. and Aki, K., 1974. *A precise, continuous measurement of seismic velocity for monitoring in situ stress*. J. Geophys. Res., *79*, 399–406.

SAIGA, A., YAMAOKA, K. and KUNITOMO, T., 2006. *Continuous observation of seismic wave velocity and apparent velocity using a precise seismic array and ACROSS seismic source*. Earth Planets Space, *58*, 993–1005.

SCHAFF, D.P. and RICHARDS, P.G., 2004. *Repeating seismic events in China*. Science, *303*, 1176–1178.

SELIN, A. and WILLIAM, J.W., 2005. *Minimum entropy time-frequency distributions*. IEEE Sig. Pro. Lett., *12*, 37–40.

SILVER, P.G., DALEY, T.M., NIU, F. and MAJER, E.L., 2007. *Active source monitoring of cross-well seismic traveltime for stress-induced changes*. Bull. Seismol. Soc. Am., *97*, 281–293.

WANG, B.S., YANG, W., YUAN, S.Y., GUO, S.J., GE, H.K., XU, P. and CHEN, Y., 2010. *An experimental study on the excitation of large volume airgun in small volume water body*. J. Geophys. Eng., *7*, 388–394.

WANG, B.S., WANG, W.T., Ge, H.K., Xu, P. and WANG, B., 2011. *Monitoring subsurface changes with active sources*. Advances in Earth Science, *26*, 249–256.

WANG, H.T., ZHUANG, S.T., XUE, B., ZHAO, C.P. and ZHU, Z.Y., 2009a. *Precisely and actively seismic monitoring*. Chinese J. Geophys., *52*, 1808–1815.

WANG, W.T., WANG, B.S., GE, H.K., CHEN, Y., YUAN, S.Y., YANG, W. and LI, Y.J., 2009b. *Using active source to monitor velocity variation in shallow sediment caused by the Wenchuan Earthquake*. Earthq. Res. in China, *25*, 223–233.

WU, C.Q., PENG, Z.G. and BEN-ZION, Y., 2009. *Non-linearity and temporal changes of fault zone site response associated with strong ground motion*. Geophys. J. Int., *176*, 265–278.

XU, Z.J. and SONG, X.D., 2009. *Temporal changes of surface wave velocity associated with major Sumatra earthquakes from ambient noise correlation*. PNAS, *106*, 14207–14212.

YANG, W., GE, H.K. and WANG, B.S., 2010. *Velocity changes observed by the precisely controlled active source for the Mianzhu M_s 5.6 earthquake*. Chinese J. Geophys., *53*, 1149–1157.

YANG, Z., LIU, B., WANG, Q., WANG, H., YUAN, S., 2011. *2-D P-wave velocity structure in the Xinfengjiang reservoir area - Results of Yingde-Heyuan-Luhe deep seismic sounding profile*. Progress in Geophys. (in Chinese), *26*(6), 1968–1975.

YAMAMURA, K., SANO, O., UTADA, H.,TAKEI, Y., NAKAO, S. and FUKAO, Y., 2003. *Long-term observation of in situ seismic velocity and attenuation*. J. Geophys. Res., *108*, B6, 2317.

YAMAOKA, K., KUNITOMO, T., MIYAKAWA, K., KOBAYASHI, K. and KUMAZAWA, M., 2001. *A trial for monitoring temporal variation of seismic velocity using an ACROSS system*. The Island Arc, *10*, 336–347.

ZHU, L.P., and RIVERA, A., 2002. *A note on the dynamic and static displacements from a point source in multilayered media*. Geophys. J. Int., *148*, 619–627.

(Received December 15, 2011, revised July 10, 2012, accepted August 23, 2012, Published online September 20, 2012)